(5) For $Cu^{II}([15]aneS_5)$, one "planar" Cu-S bond is ruptured with the four remaining Cu-S bonds requiring little rearrangement to achieve a stable tetrahedral coordination sphere.[40]

We conclude that (i) as the coordinated donor atoms undergoing bond rupture are limited to weakly held axial donor atoms and (ii) inner-sphere rearrangement is minimized, the ratio of k_{11}(Red) to k_{11}(Ox) more closely approximates unity in the current series of copper complexes. These conclusions will be examined further in future studies.

Acknowledgment. This work was supported, in part, by the National Institute of General Medical Sciences under Grant GM-20424 (to L.A.O. and D.B.R.)

Registry No. $Cu([12]aneS_4)^{2+}$, 57673-84-4; $Cu([13]aneS_4)^{2+}$, 57673-85-5; $Cu([14]aneS_4)^{2+}$, 57673-86-6; $Cu([15]aneS_4)^{2+}$, 57673-87-7; $Cu([16]aneS_4)^{2+}$, 57673-88-8; $Cu([15]aneS_5)^{2+}$, 60165-93-7; $Cu(Me_2\text{-}2,3,2\text{-}S_4)^{2+}$, 60165-82-4; $Cu(Et_2\text{-}2,3,2\text{-}S_4)^{2+}$, 57673-90-2; $Cu([12]aneS_4)^{+}$, 87464-60-6; $Cu([13]aneS_4)^{+}$, 87464-61-7; $Cu([14]aneS_4)^{+}$, 93645-98-8; $Cu([15]aneS_4)^{+}$, 87464-64-0; $Cu([16]aneS_4)^{+}$, 59918-91-1; $Cu([15]aneS_5)^{+}$, 87464-65-1; $Cu(Me_2\text{-}2,3,2\text{-}S_4)^{+}$, 87464-68-4; $Cu(Et_2\text{-}2,3,2\text{-}S_4)^{+}$, 87464-69-5; $Fe(4,7\text{-}Me_2phen)_3^{3+}$, 17378-76-6; $[Co(Me_4[14]tetraeneN_4)(H_2O)_2]^{2+}$, 38337-82-5; $Ru(NH_3)_4bpy^{2+}$, 54194-87-5; $Fe(phen)_3^{3+}$, 13479-49-7; $Fe(bpy)_3^{3+}$, 18661-69-3; $IrCl_6^{2-}$, 16918-91-5.

Contribution from the Department of Physics, The Pennsylvania State University, University Park, Pennsylvania 16802, and Departments of Chemistry, University of Notre Dame, Notre Dame, Indiana 46556, and University of Southern California, Los Angeles, California 90089-1062

Spin Coupling in Admixed Intermediate-Spin Iron(III) Porphyrin Dimers: Crystal Structure, Mössbauer, and Susceptibility Study of $Fe(TPP)(B_{11}CH_{12})\cdot C_7H_8$

Govind P. Gupta,[†‡] George Lang,*[†] Young Ja Lee,[§] W. Robert Scheidt,*[§] Kenneth Shelly,[∥] and Christopher A. Reed*[∥]

Received March 3, 1987

Susceptibility measurements on $Fe(TPP)(B_{11}CH_{12})\cdot C_7H_8$ (TPP = tetraphenylporphyrinate) in an external field of 0.2 T show that its magnetic moment varies from 2.0 to 4.2 μ_B over the temperature range 6-300 K. The data were analyzed with "Maltempo model" spins antiferromagnetically coupled within dimers. Face-to-face pairing of molecules is seen in the crystal structure. The analysis shows that the ground-state quartet $S = {}^3/_2$ (92%) is mixed with the nearby sextet $S = {}^5/_2$ (8%) through spin-orbit coupling with an unusually small coupling constant, $\xi = 150$ cm^{-1}. The exchange interaction within the dimer is estimated to be $\sim +(3.0$ cm$^{-1})\vec{S}_1\cdot\vec{S}_2$. Mössbauer spectra were recorded at temperatures varying from 4.2 to 128 K in fields 0-6 T. The chemical shift $\delta = 0.33$ mm/s (Fe) and quadrupole splitting $\Delta E_Q = 4.12$ mm/s are temperature-independent and typical of ferric ions in the admixed intermediate-spin state. Mössbauer analysis confirms the exchange interaction between the two spin systems in the dimer. The analysis also provides the rather low contact hyperfine field $P\kappa/g_N\beta_N = 8.7$ T/unit spin. The spectra imply intermediate relaxation rates even in fields of 6 T at 4.2 K, the rate increasing with increasing T and decreasing H. All Mössbauer and susceptibility data were fitted with a common parameter set; only the relaxation parameter was varied from one spectrum to another. The $[Fe(TPP)(B_{11}CH_{12})]\cdot C_7H_8$ complex is found to be five-coordinate with the carborane anion as the axial ligand with an open Fe-H-B bridge bond. The Fe-H distance is 1.82 (4) Å, and the Fe-H-B angle is 151 (3)°. The complex also has very short Fe-N bonds: the average distance is 1.961 (5) Å. The complex also exhibits an interaction between pairs of molecules suggestive of a significant π-π interaction. The separation between mean porphinato planes is 3.83 Å. Crystal data for $[Fe(TPP)(B_{11}CH_{12})]\cdot C_7H_8$: triclinic, $a = 13.660$ (2) Å, $b = 14.656$ (3) Å, $c = 13.142$ (2) Å, $\alpha = 94.85$ (1)°, $\beta = 109.63$ (1)°, $\gamma = 75.81$ (1)°, $Z = 2$, space group $P\bar{1}$, 7446 unique observed data, $R_1 = 0.079$, $R_2 = 0.092$, all observations at 293 K.

Although intermediate-spin iron(III) prophyrin complexes with apparent admixture ($S = {}^3/_2, {}^5/_2$) have been known[1] for about a decade, quantitative descriptions of their electronic structures in terms of the quantum-mechanical admixture theory of Maltempo[2] have been only partially successful.[3,4] Qualitatively, it is known that intermediate-spin states arise from highly tetragonal ligand fields, typically in five-coordinate complexes of the type Fe(Porph)Y where Y is a weak-field ligand (ClO_4^-, SbF_6^-, etc.). Room-temperature magnetic moments in the range 4.0-5.2 μ_B and $g_\perp$ values in the range 4.2-4.9 suggest widely varying degrees of admixture of $S = {}^5/_2$ character into the $S = {}^3/_2$ state although one recent interpretation dispenses with the admixture concept in favor of an empirically assigned Zeeman term g anisotropy.[5] We have accumulated variable-temperature and variable-field magnetic susceptibility and Mössbauer data on such complexes in recent years but have found a satisfactory congruence of theory and experiment only for $[Fe(OEP)(3\text{-}Cl\text{-}py)][ClO_4]$[6] and for the hexafluoroantimonate complex $Fe(TPP)(FSbF_5)\cdot C_6H_5F$.[7] The treatment in the latter case involved the use of the Maltempo model with 98% $S = {}^3/_2$ contribution to the ground state and a very small spin-orbit coupling constant ζ of 79 cm^{-1}. In addition it was necessary to postulate a nonspecific, short-range antiferromagnetic interaction that at low temperatures effectively couples all the spins of the crystal. In the present paper we find that a satisfactory treatment of Mössbauer and susceptibility data for the related carboranyl complex $Fe(TPP)(B_{11}CH_{12})\cdot C_7H_8$ can be obtained by using a Maltempo model along with pairwise intermolecular antiferromagnetic coupling. The face-to-face pairing of the five-coordinate hemes that is seen in the X-ray crystallo-

[†] The Pennsylvania State University.

[‡] On leave from the Physics Department, Lucknow University, Lucknow, India.

[§] University of Notre Dame.

[∥] University of Southern California.

(1) Dolphin, D. H.; Sams, J. R.; Tsin, T. B. *Inorg. Chem.* **1977**, *16*, 711. Masuda, H.; Taga, T.; Osaki, K.; Sugimoto, H.; Yoshida, Z.; Ogoshi, H. *Inorg. Chem.* **1980**, *19*, 950. Reed, C. A.; Mashiko, T.; Bentley, S. P.; Kastner, M. E.; Scheidt, W. R.; Spartalian, K.; Lang, G. *J. Am. Chem. Soc.* **1979**, *101*, 2948.
(2) Maltempo, M. M.; Moss, T. H. *Q. Rev. Biophys.* **1976**, *9*, 181.
(3) Spartalian, K.; Lang, G.; Reed, C. A. *J. Chem. Phys.* **1979**, *71*, 1832.
(4) Mitra, S.; Marathe, V. R.; Birdy, R. *Chem. Phys. Lett.* **1983**, *96*, 103.
(5) Ichimori, K.; Ohya-Nishiguchi, H.; Hirota, N.; Masuda, H.; Ogoshi, H. *Chem. Phys. Lett.* **1986**, *124*, 401.
(6) Gupta, G. P.; Lang, G.; Scheidt, W. R.; Geiger, D. K.; Reed, C. A. *J. Chem. Phys.* **1986**, *85*, 5212.
(7) Gupta, G. P.; Lang, G.; Reed, C. A.; Shelly, K.; Scheidt, W. R. *J. Chem. Phys.* **1987**, *86*, 5288.
(8) Gupta, G. P.; Lang, G.; Scheidt, W. R.; Geiger, D. K.; Reed, C. A. *J. Chem. Phys.* **1985**, *83*, 5945.

0020-1669/87/1326-3022$01.50/0

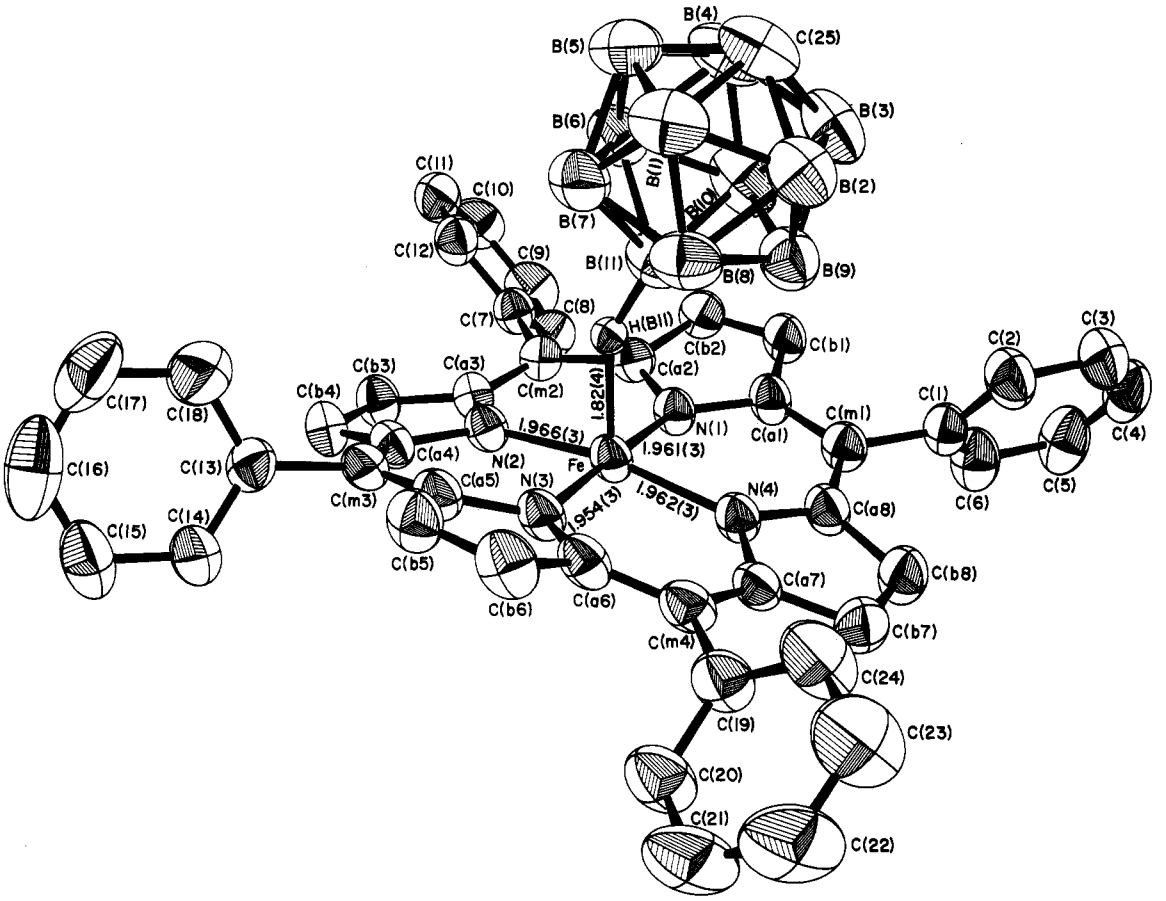

Figure 1. A computer-drawn illustration of the $[Fe(TPP)(B_{11}CH_{12})]\cdot C_7H_8$ molecule as it exists in the crystal. Ellipsoids are contoured at the 50% probability level. The atom-labeling scheme used throughout the paper is also shown. Bond distances in the coordination group are displayed. For clarity, only the hydrogen atom of the Fe–H–B bond is shown.

Table I. Summary of Crystal Data and Intensity Collection Parameters

formula	$FeN_4C_{52}B_{11}H_{48}$	cryst dimens, mm	0.33 × 0.30 × 0.90
fw	903.74	scan range	0.7 below $K\alpha_1$
space group	$P\bar{1}$		0.7 above $K\alpha_2$
temp, K	293	scan rate, deg/min	2–12
a, Å	13.660 (2)	2θ limits, deg	3.5–54.9
b, Å	14.656 (3)	radiation	graphite-monochromated Mo $K\alpha$ (λ = 0.71073 Å)
c, Å	13.142 (2)	backgd	profile analysis
α, deg	94.85 (1)	criterion for observn	$F_o > 3\sigma(F_o)$
β, deg	109.63 (1)	no. of unique obsd data	7446
γ, deg	75.81 (1)	% obsd	68
V, Å^3	2402.5	data parameter	12.3
Z	2	μ, mm^{-1}	0.35
d_{calcd}, g/cm^3	1.25	R_1	0.079
d_{obsd}, g/cm^3	1.24	R_2	0.092
scan technique	θ–2θ	goodness of fit	2.48

graphically determined structure gives considerable confidence to the interpretation and lends additional credence to the essential tenet of the Maltempo theory. This study also serves to underscore two general features that have come out of our recent work in this area.[6-9] First, it is the complementary application of magnetic susceptibility and Mössbauer studies that has led to satisfactory quantitative treatments of heme magnetic properties, and second, it is the propensity of five-coordinate hemes to associate into dimers in a crystal lattice[10] that gives many of them their more subtle and previously unrecognized magnetic and structural properties. Finally, it is of interest to probe the interplay of field strength and binding strength in weakly coordinating anions. The icosahedral carborane anion $B_{11}CH_{12}^-$ has recently appeared as a novel candidate for the least coordinating anion.[11] As such, one might expect $Fe(TPP)(B_{11}CH_{12})$ to be closest to the pure $S = {}^3/_2$ state.

Experimental Section

Fe(TPP)Br (0.40 g, 0.534 mmol) was heated to reflux in dry toluene (15 mL) within an inert-atmosphere glovebox (H_2O < 1 ppm) that was free of coordinating solvent vapors. $Ag(B_{11}CH_{12})$[12] 0.138 g, 0.550 mmol) was added and the mixture heated under reflux for 30 min. The resulting AgBr precipitate was removed by filtration through a fine-porosity frit, and hexane vapor diffusion into the filtrate gave purple crystals (0.37 g, 77%). IR (KBr): 2550 vs, 2380 m cm^{-1}, ν(B–H). UV–vis (toluene): λ_{max} 406 Soret, 500, 675 nm. The X-ray single-crystal analysis showed the presence of a 1:1 toluene solvent. Since the product is very moisture

(9) Lang, G.; Boso, B.; Erler, B. S.; Reed, C. A. *J. Chem. Phys.* **1986**, *84*, 2998.
(10) Scheidt, W. R.; Lee, Y. J. *Struct. Bonding (Berlin)* **1987**, *64*, 1.
(11) Shelly, K.; Reed, C. A.; Lee, Y. J.; Scheidt, W. R. *J. Am. Chem. Soc.* **1986**, *108*, 3117.
(12) Shelly, K.; Finster, D. C.; Lee, Y. J.; Scheidt, W. R.; Reed, C. A. *J. Am. Chem. Soc.* **1985**, *107*, 5955.

Table II. Fractional Atomic Coordinates for $[Fe(TPP)(B_{11}CH_{12})]\cdot C_7H_8$[a]

atom	x	y	z
Fe	0.44343 (4)	0.87611 (4)	0.60299 (5)
N(1)	0.46392 (24)	0.77504 (21)	0.49914 (25)
N(2)	0.57421 (24)	0.90937 (21)	0.60237 (27)
N(3)	0.41973 (26)	0.98039 (21)	0.70136 (27)
N(4)	0.29781 (24)	0.86206 (21)	0.57721 (27)
C(a1)	0.4043 (3)	0.70777 (27)	0.4649 (3)
C(a2)	0.5569 (3)	0.73895 (27)	0.4726 (3)
C(a3)	0.6382 (3)	0.87148 (27)	0.5400 (3)
C(a4)	0.6170 (3)	0.98303 (26)	0.6600 (3)
C(a5)	0.4972 (3)	1.02589 (26)	0.7659 (3)
C(a6)	0.3368 (3)	1.00700 (27)	0.7423 (4)
C(a7)	0.2189 (3)	0.91956 (26)	0.6140 (4)
C(8a)	0.2493 (3)	0.79602 (27)	0.5121 (4)
C(b1)	0.4619 (3)	0.62798 (27)	0.4214 (4)
C(b2)	0.5557 (3)	0.64666 (28)	0.4284 (3)
C(b3)	0.7133 (3)	0.92698 (29)	0.5502 (4)
C(b4)	0.7014 (3)	0.99447 (29)	0.6253 (4)
C(b5)	0.4637 (4)	1.0736 (3)	0.8527 (4)
C(b6)	0.3655 (4)	1.0629 (3)	0.8369 (4)
C(b7)	0.1205 (3)	0.8925 (3)	0.5633 (4)
C(b8)	0.1391 (3)	0.8159 (3)	0.5020 (4)
C(m1)	0.3009 (3)	0.71762 (27)	0.4656 (3)
C(m2)	0.6371 (3)	0.78662 (27)	0.4845 (3)
C(m3)	0.5870 (3)	1.03249 (26)	0.7441 (3)
C(m4)	0.2369 (3)	0.98553 (28)	0.6949 (4)
C(1)	0.2443 (3)	0.64022 (28)	0.4219 (4)
C(2)	0.2258 (4)	0.5876 (3)	0.4914 (4)
C(3)	0.1763 (4)	0.5142 (3)	0.4550 (5)
C(4)	0.1448 (4)	0.4939 (3)	0.3480 (6)
C(5)	0.1619 (4)	0.5451 (4)	0.2763 (5)
C(6)	0.2113 (4)	0.6195 (3)	0.3147 (4)
C(7)	0.7256 (3)	0.74199 (28)	0.4416 (3)
C(8)	0.7052 (3)	0.7150 (3)	0.3348 (4)
C(9)	0.7878 (4)	0.6672 (4)	0.2980 (4)
C(10)	0.8909 (4)	0.6474 (3)	0.3663 (5)
C(11)	0.9129 (4)	0.6754 (3)	0.4732 (5)
C(12)	0.8300 (3)	0.7219 (3)	0.5104 (4)
C(13)	0.6533 (3)	1.0976 (3)	0.8124 (3)
C(14)	0.6205 (4)	1.1917 (3)	0.7950 (4)
C(15)	0.6760 (5)	1.2544 (4)	0.8581 (5)
C(16)	0.7662 (6)	1.2219 (6)	0.9413 (6)
C(17)	0.8038 (5)	1.1269 (6)	0.9601 (5)
C(18)	0.7457 (4)	1.0642 (4)	0.8934 (5)
C(19)	0.1480 (4)	1.0354 (3)	0.7354 (4)
C(20)	0.1174 (4)	1.1334 (3)	0.7327 (4)
C(21)	0.0366 (5)	1.1817 (4)	0.7683 (5)
C(22)	−0.0183 (5)	1.1343 (5)	0.8087 (6)
C(23)	0.0091 (5)	1.0379 (5)	0.8111 (6)
C(24)	0.0944 (5)	0.9881 (4)	0.7761 (5)
C(25)	0.4245 (5)	0.4197 (4)	0.0420 (5)
B(1)	0.4368 (5)	0.3050 (4)	0.0012 (5)
B(2)	0.5466 (6)	0.3475 (4)	0.0853 (5)
B(3)	0.5020 (6)	0.4355 (4)	0.1700 (5)
B(4)	0.3651 (6)	0.4467 (4)	0.1391 (5)
B(5)	0.3237 (5)	0.3669 (4)	0.0345 (6)
B(6)	0.3415 (5)	0.3400 (4)	0.1669 (5)
B(7)	0.3873 (5)	0.2524 (4)	0.0827 (5)
B(8)	0.5272 (5)	0.2389 (4)	0.1137 (5)
B(9)	0.5695 (5)	0.3202 (4)	0.2198 (5)
B(10)	0.4536 (6)	0.3836 (4)	0.2520 (5)
B(11)	0.4684 (4)	0.2622 (4)	0.2168 (4)
H(C25)	0.412 (3)	0.472 (3)	−0.015 (4)
H(B1)	0.429 (3)	0.291 (3)	−0.075 (4)
H(B2)	0.605 (4)	0.354 (3)	0.054 (4)
H(B3)	0.536 (4)	0.487 (3)	0.192 (4)
H(B4)	0.320 (4)	0.521 (4)	0.140 (4)
H(B5)	0.258 (3)	0.378 (3)	−0.031 (4)
H(B6)	0.272 (3)	0.330 (3)	0.193 (4)
H(B7)	0.364 (4)	0.195 (4)	0.054 (4)
H(B8)	0.584 (4)	0.172 (3)	0.097 (4)
H(B9)	0.645 (3)	0.311 (3)	0.272 (4)
H(B10)	0.464 (3)	0.400 (3)	0.321 (4)
H(B11)	0.480 (3)	0.196 (3)	0.278 (3)

[a] The estimated standard deviations of the least significant digits are given in parentheses.

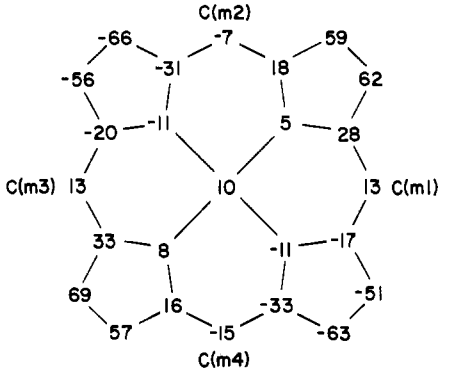

Figure 2. Formal diagram of the porphinato core showing the perpendicular displacements of each atom, in units of 0.01 Å, from the mean plane of the core.

Table III. Bond Lengths (Å) in $[Fe(TPP)(B_{11}CH_{12})]\cdot C_7H_8$[a]

Fe–N(1)	1.961 (3)	C(9)–C(10)	1.367 (7)
Fe–N(2)	1.966 (3)	C(10)–C(11)	1.382 (7)
Fe–N(3)	1.954 (3)	C(11)–C(12)	1.386 (6)
Fe–N(4)	1.962 (3)	C(13)–C(14)	1.354 (6)
Fe–H(B11)	1.82 (4)	C(13)–C(18)	1.360 (6)
N(1)–C(a1)	1.382 (4)	C(14)–C(15)	1.377 (6)
N(1)–C(a2)	1.397 (5)	C(15)–C(16)	1.356 (9)
N(2)–C(a3)	1.382 (5)	C(16)–C(17)	1.374 (9)
N(2)–C(a4)	1.398 (4)	C(17)–C(18)	1.412 (8)
N(3)–C(a5)	1.390 (5)	C(19)–C(20)	1.394 (6)
N(3)–C(a6)	1.372 (5)	C(19)–C(24)	1.370 (6)
N(4)–C(a7)	1.394 (5)	C(20)–C(21)	1.359 (7)
N(4)–C(a8)	1.379 (5)	C(21)–C(22)	1.383 (8)
C(a1)–C(m1)	1.386 (5)	C(22)–C(23)	1.371 (8)
C(a1)–C(b1)	1.433 (5)	C(23)–C(24)	1.410 (7)
C(a2)–C(m2)	1.397 (5)	B(1)–C(25)	1.706 (8)
C(a2)–C(b2)	1.428 (5)	B(1)–B(2)	1.757 (9)
C(a3)–C(m2)	1.388 (5)	B(1)–B(5)	1.761 (9)
C(a3)–C(b3)	1.425 (5)	B(1)–B(7)	1.755 (9)
C(a4)–C(m3)	1.392 (5)	B(1)–B(8)	1.755 (8)
C(a4)–C(b4)	1.423 (5)	B(2)–C(25)	1.681 (8)
C(a5)–C(m3)	1.376 (6)	B(2)–B(3)	1.762 (9)
C(a5)–C(b5)	1.435 (6)	B(2)–B(8)	1.765 (9)
C(a6)–C(m4)	1.398 (6)	B(2)–B(9)	1.752 (9)
C(a6)–C(b6)	1.425 (6)	B(3)–C(25)	1.692 (9)
C(a7)–C(m4)	1.375 (6)	B(3)–B(4)	1.744 (10)
C(a7)–C(b7)	1.421 (6)	B(3)–B(9)	1.776 (9)
C(a8)–C(m1)	1.401 (5)	B(3)–B(10)	1.744 (9)
C(a8)–C(b8)	1.424 (5)	B(4)–C(25)	1.702 (8)
C(m1)–C(1)	1.496 (5)	B(4)–B(5)	1.763 (9)
C(m2)–C(7)	1.488 (5)	B(4)–B(6)	1.762 (8)
C(m3)–C(13)	1.507 (5)	B(4)–B(10)	1.731 (10)
C(m4)–C(19)	1.492 (5)	B(5)–C(25)	1.708 (9)
C(b1)–C(b2)	1.346 (5)	B(5)–B(6)	1.740 (9)
C(b3)–C(b4)	1.357 (6)	B(5)–B(7)	1.752 (8)
C(b5)–C(b6)	1.332 (6)	B(6)–B(7)	1.761 (8)
C(b7)–C(b8)	1.349 (6)	B(6)–B(10)	1.792 (9)
C(1)–C(2)	1.366 (6)	B(6)–B(11)	1.770 (8)
C(1)–C(6)	1.359 (6)	B(7)–B(8)	1.778 (8)
C(2)–C(3)	1.377 (6)	B(7)–B(11)	1.754 (8)
C(3)–C(4)	1.355 (8)	B(8)–B(9)	1.793 (8)
C(4)–C(5)	1.363 (8)	B(8)–B(11)	1.765 (8)
C(5)–C(6)	1.393 (6)	B(9)–B(10)	1.792 (9)
C(7)–C(8)	1.379 (6)	B(9)–B(11)	1.780 (8)
C(7)–C(12)	1.383 (6)	B(10)–B(11)	1.780 (7)
C(8)–C(9)	1.386 (6)		

[a] The numbers in parentheses are the estimated standard deviations.

sensitive, all subsequent handling was done within a rigorously dry atmosphere.

Magnetic susceptibility measurements were done on a finely ground sample (ca. 0.04 g) tightly packed into an aluminum bucket that was sealed in the drybox with epoxy glue. Data were taken from 6 to 300 K in a field of 0.2 T on an SHE Model 905 SQUID susceptometer and are displayed graphically in the text. Actual data are available in Table 1S of the supplementary material.

Mössbauer spectra were gathered on a polycrystalline sample in an Apiezon L mull in a horizontal transmission geometry in the temperature

Table IV. Bond Angles (deg) in $[Fe(TPP)(B_{11}CH_{12})]\cdot C_7H_8$

N(1)FeN(2)	89.28 (12)	C(a4)C(m3)C(13)	119.1 (4)	C(25)B(3)B(9)	104.9 (4)	B(6)B(7)B(8)	109.0 (4)
N(1)FeN(3)	177.60 (14)	C(a5)C(m3)C(13)	118.4 (4)	C(25)B(3)B(10)	105.2 (5)	B(6)B(7)B(11)	60.4 (3)
N(1)FeN(4)	90.41 (12)	C(a6)C(m4)C(a7)	122.3 (4)	B(2)B(3)B(4)	107.6 (5)	B(8)B(7)B(11)	60.0 (3)
N(1)FeH(B11)	95.2 (12)	C(a6)C(m4)C(19)	118.2 (4)	B(2)B(3)B(9)	59.4 (4)	B(1)B(8)B(2)	59.9 (4)
N(2)FeN(3)	90.63 (13)	C(a7)C(m4)C(19)	119.5 (4)	B(2)B(3)B(10)	107.9 (4)	B(1)B(8)B(7)	59.6 (3)
N(2)FeN(4)	167.53 (13)	C(a1)C(b1)B(b2)	107.0 (3)	B(4)B(3)B(9)	108.5 (4)	B(1)B(8)B(9)	107.5 (4)
N(2)FeH(B11)	90.0 (12)	C(a2)C(b2)C(b1)	108.1 (3)	B(4)B(3)B(10)	59.5 (4)	B(1)B(8)B(11)	106.5 (4)
N(3)FeN(4)	89.17 (13)	C(a3)C(b3)C(b4)	107.2 (4)	B(9)B(3)B(10)	61.2 (4)	B(2)B(8)B(7)	107.0 (4)
N(3)FeH(B11)	87.2 (12)	C(a4)C(b4)C(b3)	107.6 (3)	C(25)B(4)B(3)	58.8 (4)	B(2)B(8)B(9)	59.0 (3)
N(4)FeH(B11)	102.4 (12)	C(a5)C(b5)C(b6)	107.2 (4)	C(25)B(4)B(5)	59.1 (4)	B(2)B(8)B(11)	106.0 (4)
C(a1)N(1)C(a2)	105.36 (29)	C(a6)C(b6)B(b5)	107.8 (4)	C(25)B(4)B(6)	105.1 (4)	B(7)B(8)B(9)	107.8 (4)
C(a3)N(2)C(a4)	105.2 (3)	C(a7)C(b7)C(b8)	107.9 (4)	C(25)B(4)B(10)	105.4 (4)	B(7)B(8)B(11)	59.4 (3)
C(a5)N(3)C(a6)	105.0 (3)	C(a8)C(b8)C(b7)	106.9 (4)	B(3)B(4)B(5)	108.5 (4)	B(9)B(8)B(11)	60.0 (3)
C(a7)N(4)C(a8)	105.0 (3)	B(1)C(25)B(2)	62.5 (4)	B(3)B(4)B(6)	109.6 (4)	B(2)B(9)B(3)	59.9 (4)
N(1)C(a1)C(m1)	125.5 (3)	B(1)C(25)B(3)	114.5 (4)	B(3)B(4)B(10)	60.3 (4)	B(2)B(9)B(8)	59.7 (3)
N(1)C(a1)C(b1)	110.2 (3)	B(1)C(25)B(4)	113.4 (4)	B(5)B(4)B(6)	59.1 (4)	B(2)B(9)B(10)	106.2 (5)
C(m1)C(a1)C(b1)	124.2 (3)	B(1)C(25)B(5)	62.1 (4)	B(5)B(4)B(10)	108.7 (4)	B(2)B(9)B(11)	106.0 (4)
N(1)C(a2)C(m2)	125.4 (3)	B(2)C(25)B(3)	63.0 (4)	B(6)B(4)B(10)	61.7 (4)	B(3)B(9)B(8)	107.6 (4)
N(1)C(a2)C(b2)	109.2 (3)	B(2)B(25)B(4)	113.4 (5)	C(25)B(5)B(1)	58.9 (3)	B(3)B(9)B(10)	58.6 (4)
C(m2)C(a2)C(b2)	125.3 (4)	B(2)C(25)B(5)	113.5 (4)	C(25)B(5)B(4)	58.7 (3)	B(3)B(9)B(11)	106.1 (4)
N(2)C(a3)C(m2)	125.0 (3)	B(3)C(25)B(4)	61.8 (4)	C(25)B(5)B(6)	105.8 (4)	B(8)B(9)B(10)	107.3 (4)
N(2)C(a3)C(b3)	110.1 (3)	B(3)C(25)B(5)	113.6 (4)	C(25)B(5)B(7)	105.3 (4)	B(8)B(9)B(11)	59.2 (3)
C(m2)C(a3)C(b3)	124.6 (4)	B(4)C(25)B(5)	62.2 (4)	B(1)B(5)B(4)	107.9 (5)	B(10)B(9)B(11)	59.8 (3)
N(2)C(a4)C(m3)	124.9 (4)	C(25)B(1)B(2)	58.0 (4)	B(1)B(5)B(6)	108.7 (4)	B(3)B(10)B(4)	60.2 (4)
N(2)C(a4)Ca(b4)	109.5 (3)	C(25)B(1)B(5)	59.0 (3)	B(1)B(5)B(7)	59.9 (4)	B(3)B(10)B(6)	108.2 (5)
C(m3)C(a4)C(b4)	125.3 (4)	C(25)B(1)B(7)	105.3 (4)	B(4)B(5)B(6)	60.4 (4)	B(3)B(10)B(9)	60.2 (4)
N(3)C(a5)C(m3)	125.4 (4)	C(25)B(1)B(8)	105.5 (4)	B(4)B(5)B(7)	108.4 (4)	B(3)B(10)B(11)	107.4 (4)
N(3)C(a5)C(b5)	109.5 (4)	B(2)B(1)B(5)	107.4 (4)	B(6)B(5)B(7)	60.6 (3)	B(4)B(10)B(6)	60.0 (4)
C(m3)C(a5)C(b5)	124.8 (4)	B(2)B(1)B(7)	108.4 (4)	B(4)B(6)B(5)	60.4 (4)	B(4)B(10)B(9)	108.4 (4)
N(3)C(a6)C(m4)	124.6 (4)	B(2)B(1)B(8)	60.4 (4)	B(4)B(6)B(7)	108.0 (4)	B(4)B(10)B(11)	107.1 (4)
N(3)C(a6)C(b6)	110.3 (4)	B(5)B(1)B(7)	59.8 (3)	B(4)B(6)B(10)	58.3 (4)	B(6)B(10)B(9)	108.0 (4)
C(m4)C(a6)C(b6)	125.1 (4)	B(5)B(1)B(8)	108.7 (4)	B(4)B(6)B(11)	106.2 (4)	B(6)B(10)B(11)	59.4 (3)
N(4)C(a7)C(m4)	124.6 (4)	B(7)B(1)B(8)	60.9 (4)	B(5)B(6)B(7)	60.1 (3)	B(9)B(10)B(11)	59.8 (3)
N(4)C(a7)C(b7)	109.5 (3)	C(25)B(2)B(1)	59.5 (4)	B(5)B(6)B(10)	107.0 (4)	B(6)B(11)B(7)	59.9 (3)
C(m4)C(a7)C(b7)	125.7 (4)	C(25)B(2)B(3)	58.8 (4)	B(5)B(6)B(11)	107.0 (4)	B(6)B(11)B(8)	109.1 (4)
N(4)C(a8)C(m1)	125.5 (4)	C(25)B(2)B(8)	106.1 (4)	B(7)B(6)B(10)	107.8 (4)	B(6)B(11)B(9)	109.6 (4)
N(4)C(a8)C(b8)	110.5 (3)	C(25)B(2)B(9)	106.4 (5)	B(7)B(6)B(11)	59.6 (3)	B(6)B(11)B(10)	60.6 (3)
C(m1)C(a8)C(b8)	124.0 (4)	B(1)B(2)B(3)	108.6 (5)	B(10)B(6)B(11)	59.9 (3)	B(7)B(11)B(8)	60.7 (3)
C(a1)C(m1)C(a8)	121.9 (3)	B(1)B(2)B(8)	59.8 (3)	B(1)B(7)B(5)	60.3 (4)	B(7)B(11)B(9)	109.5 (4)
C(a1)C(m1)C(1)	119.7 (3)	B(1)B(2)B(9)	109.2 (5)	B(1)B(7)B(6)	108.0 (4)	B(7)B(11)B(10)	108.7 (4)
C(a8)C(m1)C(1)	118.3 (3)	B(3)B(2)B(8)	109.5 (4)	B(1)B(7)B(8)	59.6 (4)	B(8)B(11)B(9)	60.8 (3)
C(a2)C(m2)C(a3)	121.3 (3)	B(3)B(2)B(9)	60.7 (4)	B(1)B(7)B(11)	107.0 (4)	B(8)B(11)B(10)	109.1 (4)
C(a2)C(m2)C(7)	118.6 (3)	B(8)B(2)B(9)	61.3 (3)	B(5)B(7)B(6)	59.4 (3)	B(9)B(11)B(10)	60.4 (3)
C(a3)C(m2)C(7)	120.0 (3)	C(25)B(3)B(2)	58.2 (3)	B(5)B(7)B(8)	108.0 (4)	FeH(B11)B(11)	151 (3)
C(a4)C(m3)C(a5)	122.4 (4)	C(25)B(3)B(4)	59.4 (4)	B(5)B(7)B(11)	107.1 (4)		

[a] The estimated standard deviations of the least significant digits are given in parentheses.

range 4.2–128 K and at fields varying from 0 to 6 T. Complete details of the experimental arrangements may be seen elsewhere.[13]

Crystalline $[Fe(TPP)(B_{11}CH_{12})]\cdot C_7H_8$ was subjected to preliminary examination on a Nicolet P$\bar{1}$ diffractometer. Least-squares refinement of the setting angles of 60 reflections, collected at $\pm 2\theta$, gave the cell constants reported in Table I. A Delauney reduction did not reveal any hidden symmetry. All measurements utilized graphite-monochromated Mo Kα radiation ($\bar{\lambda}$ 0.71073 Å). Details of the intensity collection procedures are also summarized in Table I. Four standard reflections were periodically measured to monitor the long-term stability of the data collection experiment. A small linear decrease ($\sim$10%) in intensity was noted as a function of X-ray exposure time. The intensity data were corrected for the decline in intensities. The structure was solved by using the direct-methods program MULTAN78.[14]

The structure was refined by full-matrix least-squares techniques; in the final anisotropic refinement cycles, the problem was segmented into three large blocks. Difference Fourier syntheses showed evidence of the location of all hydrogen atoms associated with the porphyrin ligand and the carborane anion. The hydrogen atoms of the porphinato ligand were idealized (C–H = 0.95 Å) and included as fixed contributors; however, the hydrogen atoms of the carborane ligand were refined (both coordinates and the isotropic temperature factor). The toluene solvate molecule was found to be disordered and was treated as a rigid group in the least-squars refinement. The final refined atomic coordinates are given in Table II. Final values of rigid-group parameters for the toluene solvate molecule, fixed hydrogen atom coordinates, and the final values of the anisotropic thermal parameters are given in Tables IIS–IVS of the supplementary material. Final discrepancy indices are reported in Table I.

Results and Analysis

Description of the Structure. The molecular structure of the complex is displayed in Figure 1. The figure illustrates one most salient feature, namely the presence of an axial ligand. Bond distances and angles for $[Fe(TPP)(B_{11}CH_{12})]\cdot C_7H_8$ are given in Tables III and IV, respectively. The internal agreement in the parameters of the structure is excellent.

An interesting aspect of the core conformation is shown in Figure 2. The species exhibits a near-D_{2d} ruffling of the core with substantial displacements of individual atoms from the mean plane of the 24-atom core. A stereochemical feature consonant with the substantial ruffling of the cores is the short Fe–N_p bond distances, which in turn are consistent with values expected[15] for

(13) Lang, G. *Q. Rev. Biophys.* **1970**, *3*, 1.

(14) Programs used in this study included local modifications of Main, Hull, Lessinger, Germain, Declerq, and Woolfson's MULTAN78, Jacobson's ALFF and ALLS, Busing and Levy's ORFFE and ORFLS, and Johnson's ORTEP2. Programs were run on an IBM 370/168 or a DEC VAX 11/730. Atomic form factors were from: Cromer, D. T.; Mann, J. B. *Acta Crystallogr., Sect. A: Cryst. Phys., Diffr., Theor. Gen. Crystallogr.* **1968**, *A24*, 321. Real and imaginary corrections for anomalous dispersion in the form factor of the iron atoms were from: Cromer, D. T.; Liberman, D. J. *J. Chem. Phys.* **1970**, *53*, 1891. Scattering factors for hydrogen were from: Stewart, R. F.; Davidson, E. R.; Simpson, W. T. *J. Chem. Phys.* **1965**, *42*, 3175.

(15) Scheidt, W. R.; Reed, C. A. *Chem. Rev.* **1981**, *81*, 543.

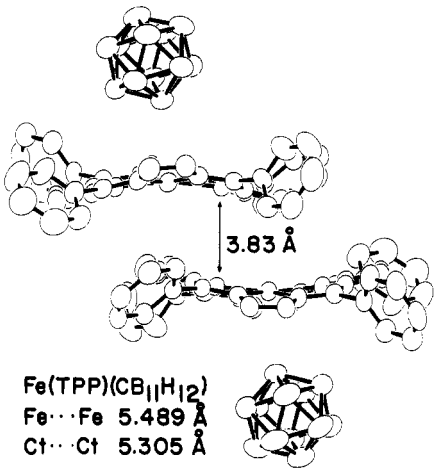

Figure 3. Edge-on view of a dimer of the $Fe(TPP)(B_{11}CH_{12})\cdot C_7H_8$ system. The Fe–H–B bond connecting the ligand to the iron atom is not shown.

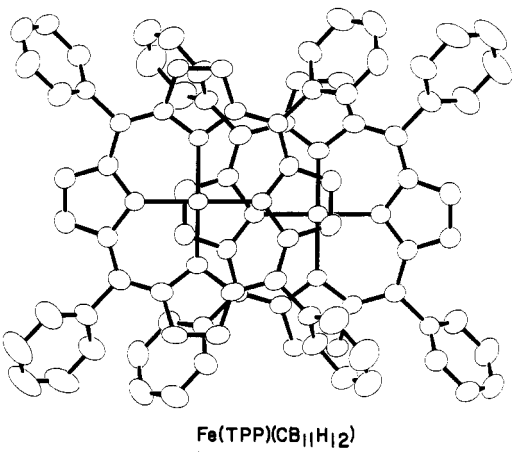

Figure 4. Projection of the two porphyrin planes within a dimer.

admixed intermediate-spin states with predominant $S = {}^3/_2$ character and not for a high-spin state. For $[Fe(TPP)(B_{11}CH_{12})]\cdot C_7H_8$, the average value is 1.961 (5) Å. This value is significantly shorter than other values found previously for admixed intermediate-spin iron(III) porphyrinates: 1.978 (3) Å in $[Fe(TPP)(FSbF_5)]\cdot C_6H_5F$,[16] 2.001 (5) Å in $[Fe(TPP)(OClO_3)]$,[17] 1.994 (23) Å in $[Fe(OEP)(OClO_3)]$,[18] 1.995 (3) Å in the polymer $[Fe(TPP)(C(CN)_3)]_n$,[19] 1.978 (12) Å in $[Fe(OEP)(THF)_2]^+$,[20] and 2.005 (6) Å in the monoclinic form of $[Fe(OEP)(3\text{-Clpy})_2]^+$.[21] Two factors in $[Fe(TPP)(B_{11}CH_{12})]\cdot C_7H_8$ lead to the decreased $Fe-N_p$ bond distances: a charge effect and a ligand effect. This species has an anionic axial ligand of rather diffuse charge. Thus the iron(III) atom has a greater charge attraction for the equatorial porphinato nitrogen atoms than in the other admixed intermediate-spin complexes listed above. Secondly, the equatorial bond distances can be taken as an indication of the tetragonality of the ligand field, consistent with the fact that the axial ligand is expected to be an exceedingly weak field ligand. As we have discussed elsewhere,[16,17] a strong tetragonal ligand field is an important factor leading to the formation of admixed intermediate-spin iron(III) porphyrinates.

Table V. Hydrogen to Carbon or Boron Distances (Å) in the $B_{11}CH_{12}^-$ Ion[a]

atom	dist	atom	dist
C(25)	1.07 (5)	B(6)	1.16 (4)
B(1)	0.98 (4)	B(7)	0.98 (5)
B(2)	1.03 (4)	B(8)	1.14 (5)
B(3)	0.96 (5)	B(9)	1.02 (4)
B(4)	1.11 (5)	B(10)	0.89 (4)
B(5)	1.00 (4)	B(11)	1.25 (4)

[a] The numbers in parentheses are the estimated standard deviations.

The short $Fe-N_p$ bond distance is coupled with a relatively small displacement of the iron atom from the mean plane of the porphinato core. The displacement from the mean plane of the core is 0.10 Å. The displacement from the plane of the four nitrogen atoms is 0.13 Å. The ordering of displacements in the known five-coordinate intermediate-spin species is different from the ordering for the $Fe-N_p$ bond distances. The displacements are significantly smaller than those observed[22] for the two perchlorato derivatives and slightly less that found for $[Fe(TPP)(FSbF_5)]\cdot C_6H_5F$. The shorter $Fe-N_p$ bonds in the current complex appear directly attributable to a smaller Ct···N size (1.955 Å) in $[Fe(TPP)(B_{11}CH_{12})]\cdot C_7H_8$. The hole sizes in the three other structurally characterized five-coordinate admixed intermediate-spin complexes are larger and essentially identical (Ct···N is 1.974 Å in $[Fe(TPP)(FSbF_5)]\cdot C_6H_5F$, 1.981 Å in $[Fe(TPP)(OClO_3)]$, and 1.977 Å in $[Fe(OEP)(OClO_3)]$). The near identity of Ct···N distances in these latter three derivatives occurs despite significant differences in core conformations. We interpret these structural data in terms of the notion that the $B_{11}CH_{12}^-$ ion is the least coordinating of the anions that have been coordinated to an iron(III) porphyrinate.

The foregoing analysis of the stereochemistry is complicated by the possibilities that the observed core conformation (vide infra) originates *solely* from intermolecular interactions and that the core conformation has *subsequent* effects on the bond lengths of the coordination group. However, we regard these possibilities as unlikely since this type of core buckling is also observed[23] in species with larger central hole sizes. We thus believe that the observed $Fe-N_p$ bond distances in these two complexes are accurate representations of the unconstrained molecules.

The five-coordinate complex interacts in pairs in the solid state. This is illustrated in Figures 3 and 4. These centrosymmetric interactions are responsible for the relatively small values of the dihedral angles between the phenyl groups and the mean plane of the core and for the particular core conformation. The values of these dihedral angles are 58.2, 44.5, 66.8, and 45.4°. In more typical metallotetraarylporphyrins, the minimum value for this dihedral angle is ~60°. The observed saddle-shaped[24] core conformation appears to be best suited to achieve the small dihedral angles needed to allow the approach of the two cores. The phenyl groups cannot become coplanar with the porphinato core because of H···H contacts of the phenyl and pyrrole hydrogen atoms. The Fe···Fe distance is 5.49 Å, and the mean separation between the two least-squares planes is 3.83 Å in $[Fe(TPP)(B_{11}CH_{12})]\cdot C_7H_8$. As can be seen from the figures, the two porphyrin cores fit together at distances less than the mean interplanar separation. Nonetheless, there are only three intermolecular contacts less than 3.5 Å. Finally, it is not obvious

(16) Shelly, K.; Bartczak, T.; Scheidt, W. R.; Reed, C. A. *Inorg. Chem.* **1985**, *24*, 4325.
(17) Reed, C. A.; Mashiko, T.; Bentley, S. P.; Kastner, M. E.; Scheidt, W. R.; Spartalian, K.; Lang, G. *J. Am. Chem. Soc.* **1979**, *101*, 2948.
(18) Masuda, H.; Taga, T.; Osaki, K.; Sugimoto, H.; Yoshida, Z.-I.; Ogoshi, H. *Inorg. Chem.* **1980**, *19*, 950.
(19) Summerville, D. A.; Cohen, I. A.; Hatano, K.; Scheidt, W. R. *Inorg. Chem.* **1978**, *17*, 2906.
(20) Masuda, H.; Taga, T.; Osaki, K.; Sugimoto, H.; Yoshida, Z.-I.; Ogoshi, H. *Bull. Chem. Soc. Jpn.* **1982**, *55*, 3891.
(21) Scheidt, W. R.; Geiger, D. K.; Hayes, R. G.; Lang, G. *J. Am. Chem. Soc.* **1983**, *105*, 2625.
(22) Values for the iron atom displacement from the 24-atom core are 0.30 Å for $[Fe(TPP)(OClO_3)]$, 0.26 Å for $[Fe(OEP)(OClO_3)]$, and 0.15 Å for $[Fe(TPP)(FSbF_5)]\cdot C_6H_5F$.
(23) A thorough analysis of core conformations and possible causes in *meso*-tetraarylporphyrin derivatives has been given elsewhere. See ref 10.
(24) In tetraarylporphyrin derivatives two idealized D_{2d} conformations are observed. One has the pyrrole rings alternatively tipped above and below the mean planes; the meso carbon atoms are located in the mean plane. This is the conformation observed here. The second has the pyrrole rings rotated along the $M-N_p$ bonds with the meso carbon atoms displaced alternatively above and below the mean plane of the core. The set of D_{2d} symmetry operators are thus rotated by 45° in two cases.

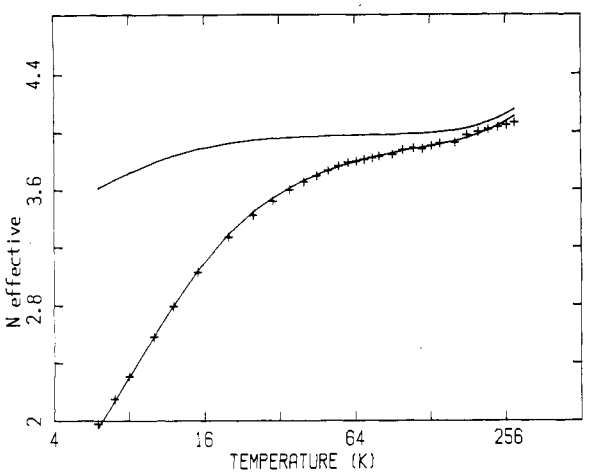

Figure 5. Experimental values (+) of N_{eff} as a function of temperature, where $N_{eff} = 3kT\chi/\beta^2$ and χ is the susceptibility per heme unit. The data are fitted (shown as the solid curve) with the parameters $g = 4.15$, $\zeta = 150$ cm^{-1}, and $J = -3.0$ cm^{-1} by using (1). The top curve corresponds to $J = 0$.

whether particular core–core interactions are responsible for the strongly developed dimeric interaction in $[Fe(TPP)(B_{11}CH_{12})]\cdot C_7H_8$ and other dimeric porphinato species. We also note that the importance of this type of saddle-shaped core complex for the MTPP π cation radicals has been given elsewhere.[9,10,25]

$[Fe(TPP)(B_{11}CH_{12})]\cdot C_7H_8$ presents a quite interesting result in the coordination chemistry of iron(III) porphyrinates, namely, a new solution for the extreme avidity of $[Fe(TPP)]^+$ for an axial ligand. As can be seen in Figure 1, the $B_{11}CH_{12}^-$ anion coordinates to the iron(III) atom through an open Fe–H–B bond. Although unsupported metal–hydrogen–boron bonds are very rare,[26,27] several features suggest a real interaction between the "soft" carborane and the "hard" iron(III) porphyrinate. First is the fact that the closest boron atom is opposite the carbon atom of the icosohedron and thus has the most "hydridic" B–H bond of the carborane. Second, the behavior of the carborane hydrogen atoms in the crystal structure refinement was that expected for a bridge bond. In order to obtain Fe–H and B–H distances adequate to judge the interaction, the hydrogen atom coordinates and an isotropic temperature factor were refined. Final derived B–H and C–H bond distances are reported in Table V. As expected, the B(11)–H distance of 1.25 (4) Å is longer than any other in the cluster. The Fe–H bond distance is 1.82 (4) Å. These values can be compared with the Fe–H and B–H distances found in a series of ferraboranes with Fe–H–B interactions: 1.56 (5) and 1.37 (5) Å in $HFe_4(CO)_{12}BH_2$,[28] 1.61 (4) and 1.32 (4) Å in $B_3H_7Fe_2(CO)_6$,[29] and a Fe–H distance of 1.56 (6) Å in $Cu[P(C_6H_5O)_3]_2B_5H_8Fe(CO)_3$.[30] It is seen that the B–H distances compare quite well; the Fe–H distances are generally shorter. This is in keeping with the high oxidation state of the central iron in the complex. The Fe–H–B angle in $[Fe(TPP)(B_{11}CH_{12})]\cdot C_7H_8$ is 151 (3)°, much larger than the ~120° value usually[26] observed. A value greater than 120° might be required to avoid nonbonded interactions between the anion and the cation although it appears that an angle smaller than 150° would be possible without causing unreasonably short nonbonded contacts.

Susceptibility. The susceptibility of $Fe(TPP)(B_{11}CH_{12})\cdot C_7H_8$ was measured at 0.2 T in the extended temperature range of 6–300 K. The effective number of Bohr magnetons, N_{eff}, has been plotted vs. temperature in Figure 5. Since N_{eff} decreases rapidly at low temperature when zero-field splitting becomes important, the temperature scale has been chosen to be logarithmic. The N_{eff} value climbs rapidly from 2.0 at 6 K, levels to about 3.9 at 100 K, and then climbs again at higher temperatures. Such behavior is typical of complexes believed to have quantum-mechanical admixed intermediate-spin states.[4,6,7]

The data shown in Figure 5 were compared with the "Maltempo model" by use of the following Hamiltonian for the coupled spin-pair of a dimer:[6]

$$\mathcal{H}_{el} = \sum_{1,2}[\Delta + \zeta\sum_i l_i s_i + 2\beta\vec{H}\cdot\vec{S}] - J\vec{S}_1\cdot\vec{S}_2 \qquad (1)$$

where the terms in square brackets pertain to individual iron sites. Inside the brackets, the first term (Δ) is the energy gap between $S = {}^3/_2$ and $S = {}^5/_2$ spin states, the second term represents the spin–orbit interaction with ζ as its one-electron-coupling constant (summation over i is extended over all five 3d electrons of the ferric ion), and the last term is the Zeeman interaction of the electronic spin S ($=\sum s_i$) with the external field H. J parameterizes the exchange interaction between the neighboring spins S_1 and S_2 of the dimer.

The energy separation Δ may be related to the transverse gyromagnetic ratio $g_\perp$ of the lowest doublet, $S_z = \pm{}^1/_2$, by

$$\Delta = \pm\zeta\left[-\frac{24(g_\perp - 5)^2}{5(g_\perp - 6)(g_\perp - 4)}\right]^{1/2} \qquad (2)$$

where the lower sign applies for $g_\perp < 5$. Normally $g_\perp$ is proportional to the magnetic splitting of the ground doublet and may be directly measured by EPR. However, in the present case the Kramers degeneracy is destroyed because of the exchange interaction term and no EPR signal is expected. g may be considered simply as a parameter indicating the percentage of spin state $S = {}^3/_2$ in the admixed spin state. The values of $g_\perp$ are linearly related to this percentage[2] with boundary values 0 and 100% corresponding to $g_\perp = 6$ and 4, respectively.

Theoretical values of N_{eff} obtained by using the parameters $g_\perp = 4.15$, $\zeta = 150$ cm^{-1}, and $J = -3.0$ cm^{-1} are in excellent agreement with the experimental measurements as shown in Figure 5. As discussed in an earlier paper,[6] the estimation of the three parameters is unique to a large extent. The middle part of the susceptibility curve (60–100 K), where N_{eff} levels off, is much more sensitive to $g_\perp$ as compared with the other two parameters. For a given $g_\perp$, the high-temperature part could be fitted by varying ζ alone, because an antiferromagnetic exchange interaction of the order of few reciprocal centimeters does not appreciably affect the susceptibility at high temperature. Once $g_\perp$ and ζ are estimated, the low-temperature part of the curve may be fitted by varying the value of J. The sharp fall of the susceptibility at low temperature is a decisive indication of the presence of an antiferromagnetic exchange interaction between the spins of the dimers. A susceptibility curve for uncoupled hemes ($J = 0$) is also shown in Figure 5 for comparison. If the high-temperature part of the N_{eff} curve is ignored, there is usually a tradeoff between ζ and $-J$ at low temperature. However, in the present case, the effect of ζ is close to saturation, and increasing it further has minimal effect in bringing the curve down. Thus, there is no alternative but to introduce $-J$ in order to match the experimental data. This relatively unique estimation of parameters is strictly within the Maltempo model a priori assumption of axial symmetry. This is not restrictive in the present case since there is clearly an effectively isolated quartet ground state. Such a state has inherent axial symmetry.

Mössbauer Spectra in Zero Field. Mössbauer spectra were recorded in zero field at 4.2 and 77 K. Quadrupole doublets observed in both cases were fitted by using a least-squares minimization routine[31] with Lorentzian line width, isomer shift δ, and

(25) Erler, B. S.; Scholz, W. F.; Lee, Y. J.; Scheidt, W. R.; Reed, C. A. *J. Am. Chem. Soc.* **1987**, *109*, 2644.
(26) Teller, R. G.; Bau, R. *Struct. Bonding (Berlin)* **1981**, *44*, 1–82.
(27) An example of such a bond in a formal iron(II) complex, $[FeH(dmpe)_2(BH_4)]$, has been recently reported: Baker, M. V.; Field, L. D. *J. Chem. Soc., Chem. Commun.* **1984**, 996.
(28) Fehlner, T. P.; Housecroft, C. E.; Scheidt, W. R.; Wong, K. S. *Organometallics* **1983**, *2*, 825.
(29) Haller, K. J.; Anderson, E. L.; Fehlner, T. P. *Inorg. Chem.* **1981**, *20*, 309.
(30) Mangion, M.; Ragaini, J. D.; Schmitkons, T. A.; Shore, S. G. *J. Am. Chem. Soc.* **1979**, *101*, 754.
(31) Lang, G.; Dale, B. W. *Nucl. Instrum. Methods* **1974**, *116*, 567.

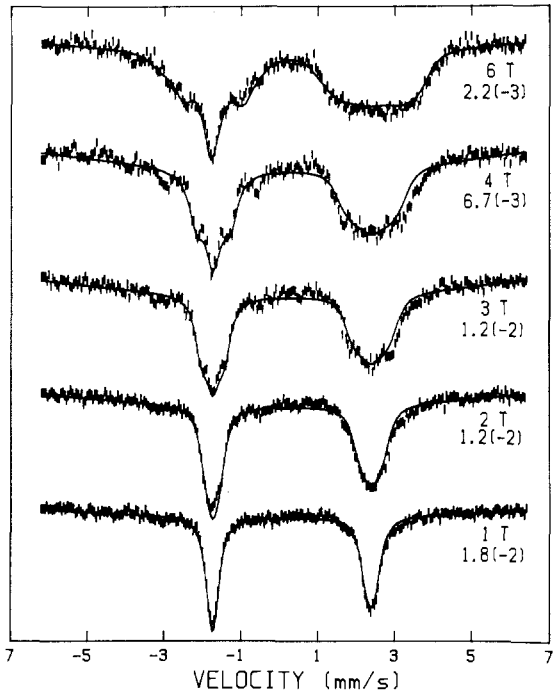

Figure 6. Mössbauer spectra at 4.2 K in various fields as shown. The solid curves are the corresponding simulated spectra with $g = 4.15$, $\zeta = 150$ cm^{-1}, $J = -3.0$ cm^{-1}, $\Delta E_Q = 4.12$ mm/s, $\delta = 0.33$ mm/s, $P/g_N\beta_N = 48.5$ T/unit spin, and $\kappa = 0.18$. Relaxation rates w_0 in mm/(s cm^3) are also shown in the figure along with fields for each spectrum. The numbers in the parentheses are the powers of 10 as a multiplying factor.

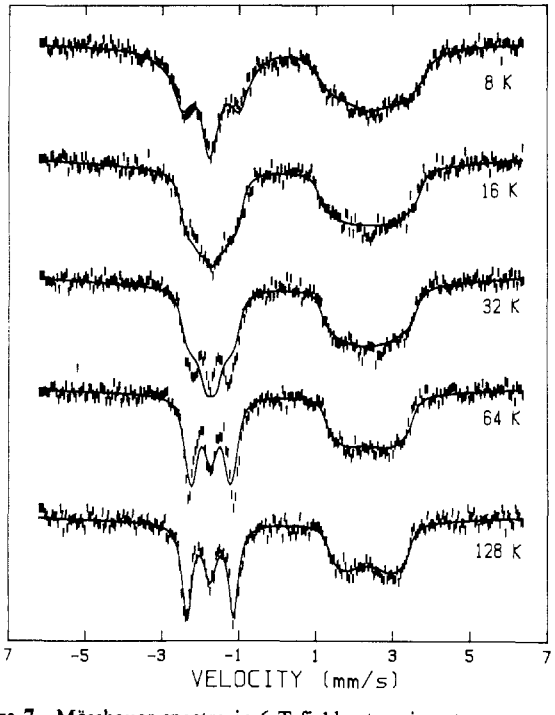

Figure 7. Mössbauer spectra in 6-T fields at various temperatures as shown. The simulated spectra (solid curves) are calculated by using parameters given in Figure 6. Only the 8 K spectrum is fitted in the intermediate relaxation regime with $w_0 = 0.001$ mm/(s cm^{-3}). Other spectra are fitted in the fast relaxation limit.

quadrupole splitting ΔE_Q as free parameters. The values of line width, 0.30 mm/s, and quadrupole splitting, 4.12 mm/s, are independent of temperature within experimental accuracy. The value of δ, 0.33 mm/s at 4.2 K, is that expected for iron in the ferric state. The large quadrupole splitting of 4.12 mm/s is very suggestive of its admixed intermediate-spin state as discussed later.

Mössbauer Spectra in Fields. Mössbauer spectra recorded at 4.2 K in various fields are shown in Figure 6, and those at higher temperatures in 6 T are shown in Figure 7. The spectra were fitted by solving the electronic and nuclear Hamiltonians separately. This holds true if the applied fields are strong enough to decouple electronic and nuclear spins, i.e., greater than 1 mT or so. Assuming axial symmetry, the electronic Hamiltonian was diagonalized for 10 equally weighted orientations of the molecule with respect to the applied field in order to carry out the simulations for a polycrystalline sample.

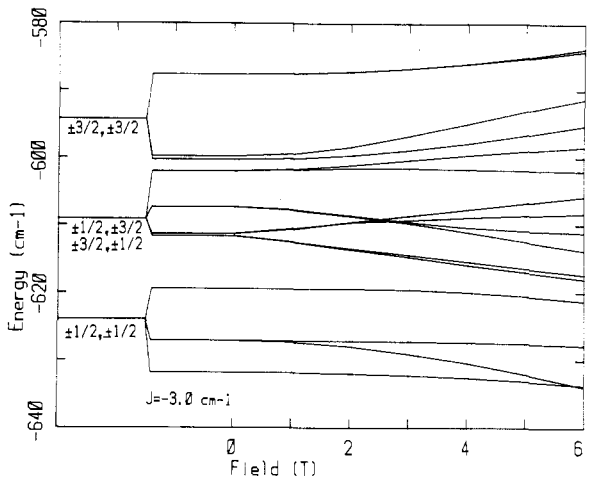

Figure 8. Energy level diagram for the lowest 16 spin states of an iron–iron pair in Fe(TPP)($B_{11}CH_{12}$)·C_7H_8 corresponding to $g = 4.15$, $\zeta = 150$ cm^{-1}, and $J = -3.0$ cm^{-1}. The other higher states, not shown in the diagram, are more than 500 cm^{-1} above these levels. At the right is shown the effect of a field applied in the x–y plane.

Once the electronic problem is solved for different orientations, the three components of hyperfine field for each energy level are calculated as the expectation values of

$$H_{x,y} = (P/g_N\beta_N)\cdot(\alpha/2 + \kappa)\cdot S_{x,y}$$
$$H_z = (P/g_N\beta_N)\cdot(-\alpha + \kappa)\cdot S_z \quad (3)$$

where P and κ are the hyperfine and contact constants, respectively, and α is the dipolar contribution, which is zero for ^{6}S and $^8/_{21}$ for ^{4}A states of the Maltempo model.[2] The matrix elements of orbital contribution to the hyperfine field are zero.

The spectra were fitted with a modification of a computer program written by Schulz and co-workers[32] as discussed in our earlier papers.[6,7] At 4.2 K, since only low-lying energy levels are occupied, the direct relaxation processes[33,34] were considered among four low-lying energy levels that are basically formed as a result of coupling $S_z = \pm^1/_2$ levels of the two neighboring Fe ions in the dimers. Since coupling renders this system to be non-Kramers, following the procedures described in ref 6, the spectra were fitted with the relaxation parameter

$$W_0 = 3V_0^2/(2\pi\hbar^4 v^5\rho) \quad (4)$$

as the only adjustable variable. Here V_0 is the average dynamic crystal potential of the first order, v is the velocity of sound in the medium, and ρ is its density. Since the observable effect of relaxation is to broaden the Mössbauer absorption lines, we prefer to define $w_0 = h^4c^4W_0/E_\gamma$, where E_γ is energy of the Mössbauer γ ray (14.36 keV), and to specify w_0 in units of mm/(s cm^3). This is convenient when the Mössbauer energy scale in mm/s is used and the electronic level separation is known in cm^{-1}.

Unlike those of the other systems,[6,7] the 4.2 K 6-T spectrum in this case could not be fitted in the slow relaxation limit. The effect may be attributed to the large degree of antiferromagnetic

(32) Winkler, H.; Schulz, C.; Debrunner, P. G. *Phys. Lett. A* **1979**, *69A*, 360. See also: Schulz, C. Ph.D. Thesis, University of Illinois, 1979.
(33) Orbach, R.; Stapleton, H. J. *Electron Paramagnetic Resonance*; Geschwind, S., Ed.; Plenum: New York, 1972; p 121.
(34) Orbach, R.; *Proc. R. Soc. London, A* **1961**, *264*, 458.

Table VI. Values of Various Parameters As Discussed in the Text for Different Five-Coordinated Iron(III) Porphyrin Derivatives

complex	$g_\perp$	% $S = {}^3/_2$	δ, mm/s	ΔE_Q, mm/s	J, cm^{-1}	$P\kappa/g_N\beta_N$, T/unit spin	ζ, cm^{-1}	MPS, Å	Fe–Fe, Å	ref
(1) $[FeCl(TPP^\bullet)]^+$	6	0	0.39	0.56	−0.6[a]	17.1				9
(2) [Fe(OEP)(2-MeHIm)][ClO_4]	5.95	2	0.40	1.39	−0.8	17.4	300	3.31	4.28	8
(3) [Fe(OEP)(3-Cl-py)][ClO_4]	4.38	81	0.36	3.23	−0.4	12.7	150	3.51	5.14	6
(4) Fe(TPP)($B_{11}CH_{12}$)·C_7H_8	4.15	92	0.33	4.12	−3.0	8.7	150	3.83	5.49	this work
(5) Fe(TPP)($FSbF_5$)·C_6H_5F	4.05	98	0.39	4.29	−1.4[b]	7.0	50			7

[a] This is probably a dimer but structural data are known only for the *p*-tolyl analogue (MPS = 4.7 Å, Fe–Fe = 5.4 Å). [b] This is not a dimer. J must be reduced by a factor $1/n$ for comparison with other cases where n is the number of coupled neighboring spins.

exchange interaction present between spins of the dimers in this system. The point may be explained by the help of the energy level diagram shown in Figure 8, which depicts the behavior of 16 low-lying energy levels. Other energy states are more than 500 cm^{-1} above these levels and may be ignored. The 16 levels are basically formed as a result of coupling $S_z = \pm{}^1/_2$ and $S = \pm{}^3/_2$ levels of the two spins of the dimers. At 4.2 K, only the lowest four levels will be populated. These comprise two singlets and a middle degenerate doublet in the presence of the antiferromagnetic coupling. In the presence of an external field applied in the x–y plane (which is statistically most effective) the middle doublet splits and its lower member develops a large magnetic moment (represented by its slope) and crosses the ground singlet just before 6 T (see Figure 8). At 6 T, the two lowest levels are almost equally populated at 4.2 K and direct relaxation between them takes place. In previous cases (see for example Figure 8 of ref 6), the value of $-J$ is small, the level crossing is near 1 T, and by 6 T only the strongly magnetic level is populated at 4.2 K. Thus, intermediate relaxation and lack of large magnetic features in the Mössbauer spectrum at 4.2 K and 6 T are indications of large $-J$. This in turn makes it difficult to determine appropriate values of the hyperfine parameters P and κ for the spectrum. By a trial and error method, the 4.2 K 6-T spectrum was fitted with $P/g_N\beta_N = 48.5$ T/unit spin, $\kappa = 0.18$, and $w_0 = 0.0022$ mm/(s cm^3).

All other spectra shown in Figure 6 were well simulated by using a common set of parameters except for the relaxation rate, which was found to be monotonic in field. The various rates that minimize the mean-square error are also shown in Figure 6. The low-field spectra are of particular interest. Up to 2 T there is hardly any magnetic structure, a strong indication that the ground state is a singlet located well below any degenerate levels. This qualitative feature is diagnostic of the antiferromagnetic coupling by pairs, with $-J$ of order of 4 K.

Mössbauer spectra recorded in 6 T at higher temperatures, shown in Figure 7, could also be fitted with the same set of parameters. However, the agreement between theoretical and experimental spectra becomes progressively worse as the temperature is increased. This effect may be attributed to the fact that more than four energy levels become involved in the relaxation process at higher temperatures. As shown in Figure 8, the other levels are within a few reciprocal centimeters of the lowest four, which themselves are spread over 12 cm^{-1} or so. Thus, the assumption that only four energy levels are populated holds reasonably well only up to 8 K. Computation of Mössbauer spectra with an intermediate rate of relaxation involving more energy levels is unduly expensive in terms of computer time and was avoided. The 8 K spectrum could be fitted reasonably well with the relaxation parameter $w_0 = 0.001$ mm/(s cm^3) as shown in Figure 7.

All other spectra shown in Figure 7 were fitted in the fast relaxation limit by using the modified program of Lang and Dale[31] considering all 16 energy levels shown in Figure 8. The agreement improves as the temperature is increased, but only in the 128 K spectrum is the fast relaxation limit reached. By this temperature, the induced average moment is very small, and the spectrum is essentially determined by the direct effect of the applied field on the nucleus.

Discussion

The foregoing analysis of the susceptibility and Mössbauer data for Fe(TPP)($B_{11}CH_{12}$)·C_7H_8 provides a good agreement of experiment and theory. Confidence in the basic description as a 92:8 $S = {}^3/_2, {}^5/_2$ admixed state with pairwise antiferromagnetic coupling comes from the use of a common parameter set for fitting data derived from complementary techniques and from the observation of face-to-face dimerization in the crystal lattice. A reviewer has asked us to comment on the relatively small values of ζ, P, and κ. We note that we have taken an approach which is essentially that of the crystal field treatment and we adjust ζ, P, and κ to fit our results. A much more refined molecular orbital approach, which might determine their values and their variation from one spin state to another, is beyond our present scope, apart from rough arguments such as those given in the discussion of ref 6. We would hope that publication of our results might stimulate some interest on the part of specialists is this area.

The magnitude of the intermolecular spin coupling in Fe(TPP)($B_{11}CH_{12}$)·C_7H_8 ($J = -3.0$ cm^{-1}) is notable. It is by far the strongest we have observed in crystalline iron porphyrin complexes in spite of a relatively large iron–iron separation. Table VI lists relevant parameters for the five iron(III) complexes that we have investigated in detail. All are five-coordinate compounds, and all are magnetically coupled. Entries 2–4 are directly comparable since all are known to crystallize as face-to-face dimers. Surprisingly, the present complex (entry 4) has the strongest interaction (as measured by the magnitude of J) but also the largest iron–iron separation. The mean plane separation (MPS) also shows no correlation with the magnitude of the spin coupling. This suggests that less identifiable features such as the precise orientation of the porphyrin cores relative to each other (see Figure 4) and the degree of delocalization of spin density from iron onto the porphyrin ring may be as important as simple spatial separation. We note that in the present structure the out-of-plane displacement of the iron atom (0.11 Å) is the smallest and may allow the greatest spin delocalization. We also note that there is a theoretical basis for the expectation of an inverse proportionality of $|-J|$ and the number of unpaired electrons.[35] All other factors being equal, lower multiplicity spin systems are expected to show stronger coupling.

Despite the present lack of a quantitative correlation of spin coupling with structure, it is clear that magnetic coupling of the order of a wavenumber is now an expectation in five-coordinate iron porphyrins, and possibly for other paramagnetic porphyrin complexes as well. It is a feature of all pentacoordinate complexes that we have investigated to date and is associated with dimerization in four of the five cases. The fifth entry in Table VI lists data for Fe(TPP)($FSbF_5$)·C_6H_5F, which does not dimerize and whose properties cannot be rationalized by a pairwise interaction model. Rather, a nonspecific lattice interaction model was developed.[7] The value of J in this case (−1.4 cm^{-1}) is not directly comparable and must be reduced by a factor of $1/n$ where n is the number of nearest-neighbor spins. In practice, such systems do not have the easily identifiable Mössbauer signature of spin coupling shown by the dimers, but careful analysis does make it detectable. Susceptibility results for high-spin Fe(TPP)Cl have been analyzed in terms of very weak dimer coupling with interaction (−0.28 cm^{-1})$S_{1z}S_{2z}$ + (0.106 cm^{-1})($S_{1x}S_{2x} + S_{1y}S_{2y}$).[36]

A distinctive feature of complexes that can be described as $S = {}^3/_2, {}^5/_2$ admixtures is their large quadrupole splittings. An

(35) Hay, P. J.; Thibeault, J. C.; Hoffmann, R. *J. Am. Chem. Soc.* **1975**, *97*, 4884.
(36) Neiheisel, G. L.; Imes, J. L.; Pratt, W. P. *Phys. Rev. Lett.* **1975**, *35*, 101.

inspection of Table VI reveals that ΔE_Q values increase steadily as the precentage of $S = {}^3/_2$ character increases. We have noted previously the correlation of large ΔE_Q with small spin-orbit coupling (ζ) and small hyperfine field ($P\kappa/g_N\beta_N$).[5,7] The results suggest that the carborane ligand is a stronger field ligand than hexafluoroantimonate since they analyze for 92 and 98% $S = {}^3/_2$, respectively. This is interesting because viewing their structures solely in the context of spin state would lead to the opposite conclusion. The Fe-N bond lengths and the Fe out-of-plane displacements[11] are smaller for the carborane than for the hexafluoroantimonate, as expected for a *lower* $S = {}^5/_2$ contribution. An explanation lies in the interplay of field strengths and binding strength and reminds us that these factors are not synonymous nor necessarily correlated. The p_π donor capability of the fluoride donor apparently makes SbF_6^- a weaker field ligand than $B_{11}CH_{12}^-$ despite the stronger binding indicated in the structural comparison. The carborane is not capable of p_π donation. If the two anions were hypothetically assumed to have equal σ-donor interactions, then the SbF_6^- coordination parameters would be expected to be the same as or *smaller than* $B_{11}CH_{12}^-$. That they are larger indicates that the σ-donor interaction of SbF_6^- is considerably greater than that of $B_{11}CH_{12}^-$. This further supports the hypothesis[11] that $B_{11}CH_{12}^-$ is the lesser coordinating of these two anions.

In summary, a combination of susceptibility and Mössbauer studies and a knowledge of structure lead to a good quantitative description of the magnetic properties of intermediate-spin iron(III) porphyrins. Previously unrecognized intermolecular antiferromagnetic coupling of moderate magnitude seems to be the rule rather than the exception in five-coordinate complexes, particularly when association into dimers occurs in the crystal lattice. The question of spin coupling among six-coordinate porphyrin complexes remains open since coupling involving more than a pair of lattice sites does not provide an easily identified signature in the Mössbauer spectrum.

Acknowledgment. We thank the National Institutes of Health for support of this work under Grants HL-16860 (G.L.) and GM-38401 (W.R.S.) and the National Science Foundation for the support under Grant CHE85-19913 (C.A.R.).

Registry No. $[Fe(TPP)(B_{11}CH_{12})]\cdot C_7H_8$, 102149-51-9; Fe(TPP)Br, 25482-27-3.

Supplementary Material Available: For $[Fe(TPP)(B_{11}CH_{12})]\cdot C_7H_8$, Table IS (magnetic measurements), Tables IIS and IIIS (fixed atomic coordinates), and Table IVS (anisotropic temperature factors) (5 pages); a listing of observed and calculated structure amplitudes (×10) (25 pages). Ordering information is given on any current masthead page.

Contribution from the Department of Chemistry and the Molecular Structure Center, Indiana University, Bloomington, Indiana 47405

Direct Synthesis of VE^{2+} (E = S, Se) Complexes Using Elemental Chalcogens. Preparation, Structure, and Properties of $[VS(SPh)_4]^{2-}$ and $[VSe(edt)_2]^{2-}$ (edt^{2-} = Ethane-1,2-dithiolate)

John R. Nicholson,[1a] John C. Huffman,[1b] Douglas M. Ho,[1b] and George Christou*,†,[1a]

Received April 7, 1987

The reaction of elemental sulfur or selenium with VCl_3/sodium thiolate reaction mixtures in MeCN provides a convenient and direct route to mononuclear complexes containing the VE^{2+} (E = S, Se) moiety. The preparation of complexes containing the $[VS(SPh)_4]^{2-}$, $[VSe(SPh)_4]^{2-}$, or $[VSe(edt)_2]^{2-}$ dianion is described. $[PhCH_2NMe_3]_2[VS(SPh)_4]$ (**1**) crystallizes in monoclinic space group $P2_1$ with unit cell dimensions (at −156 °C) of a = 10.312 (4) Å, b = 16.293 (6) Å, c = 13.930 (6) Å, β = 117.57 (2)°, and Z = 2. The anion contains a vanadium(IV) center in its characteristic square-pyramidal geometry with a multiply bonded S atom in the apical position and four benzenethiolate S atoms in the basal positions. The V=S bond length is 2.078 (2) Å. $(NEt_4)_2[VSe(edt)_2]$ (**3**) crystallizes in orthorhombic space group $P2_1ab$ with unit cell dimensions (at −155 °C) of a = 15.005 (4) Å, b = 12.769 (3) Å, c = 14.248 (3) Å, and Z = 4. Again, the vanadium(IV) center has square-pyramidal geometry with a multiply bonded Se atom in the apical position and four thiolate S atoms from two chelating edt^{2-} groups occupying the basal positions. Complex **3** is the first structurally characterized example of a VSe^{2+} species. The V=Se bond length is 2.196 (3) Å. Complex **1** is only the third example of a structurally characterized VS^{2+} species. A linear relationship has been found to exist between the bond length and the IR stretching frequency of the the V=S unit.

Introduction

Research in this group is directed toward the development of discrete metal-sulfide-thiolate chemistry for an early 3d transition metal, namely vanadium. Preliminary progress has been the subject of several recent reports,[2-7] and we now have V/S/SR species spanning the oxidation level range III-V and nuclearities of 1-4. In one of these reports[2] we described how the oxovanadium(IV) complex $[VO(edt)_2]^{2-}$ could be converted to the sulfur analogue $[VS(edt)_2]^{2-}$ by treatment with $(Me_3Si)_2S$. While pure product was obtained, its yield was relatively low (34%) and, of course, this procedure required prior preparation of the oxo complex. As we continued to extend our studies of V/S/SR chemistry, it was recognized that a direct synthetic route to thiovanadium(IV) complexes could make available large quantities and allow future reactivity studies of these highly reactive materials to be more conveniently performed. We thus decided to seek such a direct synthetic procedure and herein report the results of this search. As we describe below, this objective has been realized. We have also extended it and developed a direct route to complexes containing the extremely rare $[V{=}Se]^{2+}$ unit, and describe the first structural characterization of such a species.

Experimental Section

Syntheses. All manipulations were performed by using standard inert-atmosphere techniques and a purified dinitrogen atmosphere. MeCN (CaH_2) and Et_2O (Na/benzophenone) were purified by distillation and thoroughly degassed before use. Dry NaSPh and Na_2edt were prepared

† Alfred P. Sloan Research Fellow, 1987-1989.

(1) (a) Department of Chemistry. (b) Molecular Structure Center.
(2) Money, J. K.; Huffman, J. C.; Christou, G. *Inorg. Chem.* **1985**, *24*, 3297.
(3) Money, J. K.; Folting, K.; Huffman, J. C.; Collison, D.; Temperley, J.; Mabbs, F. E.; Christou, G. *Inorg. Chem.* **1986**, *25*, 4583.
(4) Money, J. K.; Nicholson, J. R.; Huffman, J. C.; Christou, G. *Inorg. Chem.* **1986**, *25*, 4072.
(5) Money, J. K.; Huffman, J. C.; Christou, G. *J. Am. Chem. Soc.* **1987**, *109*, 2210.
(6) Money, J. K.; Folting, K.; Huffman, J. C.; Christou, G. *Inorg. Chem.* **1987**, *26*, 944.
(7) Money, J. K.; Huffman, J. C.; Christou, G., submitted for publication.

0020-1669/87/1326-3030$01.50/0